Heliyon 7 (2021) e08119

Contents lists available at ScienceDirect

Heliyon

journal homepage: www.cell.com/heliyon

Research article

Cerebellar nuclei neurons display aberrant oscillations during harmaline-induced tremor

Yuval Baumel, Hagar G. Yamin, Dana Cohen *

The Leslie and Susan Gonda Multidisciplinary Brain Research Center, Bar-Ilan University, Ramat-Gan, 52900, Israel

ARTICLE INFO

Keywords:
Oscillations
CN
Synchrony
Chronic recordings
Harmaline
DCN
Essential tremor
Coherence
Electrophysiology
Neuronal activity

SUMMARY

Essential tremor, a common, debilitating motor disorder, is thought to be caused by cerebellar malfunction. It has been shown that rhythmic Purkinje cell firing is both necessary and sufficient to induce body tremor. During tremor, cerebellar nuclei (CN) cells also display oscillatory activity. This study examined whether rhythmic activity in the CN characterizes the occurrence of body tremor, or alternatively, whether aberrant bursting activity underlies body tremor. Cerebellar nuclei activity was chronically recorded and analyzed in freely moving and in harmaline treated rats. CN neurons displayed rhythmic activity in both conditions, but the number of oscillatory neurons and the relative oscillation time were significantly higher under harmaline. The dominant frequencies of the oscillations were broadly distributed under harmaline and the likelihood that two simultaneously recorded neurons would co-oscillate and their oscillation coherence were significantly lower. It is argued that these alterations rather than neuronal rhythmicity per se underlie harmaline-induced body tremor.

1. Introduction

Oscillations at different dominant frequencies occur throughout the brain and are thought to play a prominent role in global information processing (Buzsaki, 2006; Mazzoni et al., 2008; Sohal et al., 2009; Van Wingerden et al., 2010; Buschman and Miller, 2009; Ribary, 2005; Kayser et al., 2009). Neuronal oscillations occur at all levels of the movement production network including cortical regions, deep brain structures and spinal motoneurons (Kiehn and Kjaerulff, 1998; Conway et al., 1995; Donoghue et al., 1998; Gross et al., 2002; Williams et al., 2010). In many cases, deviations from normally occurring oscillations are believed to underlie impaired motor performance (Brown, 2006; Mallet et al., 2008; Pinault et al., 2001; Muthuraman et al., 2012; Kondylis et al., 2016).

The cerebellar cortex supports oscillatory activity occurring at a broad range of frequencies even in the absence of movement (Courtemanche et al., 2002, 2013; Levesque et al., 2020). However, the occurrence of oscillations in the cerebellar nuclei remains controversial. Oscillations have been observed in the CN during smooth slow (0.5Hz) finger movements in humans and has been suggested to underlie the 6–9 Hz discontinuities detected in muscle activity during these movements (Gross et al., 2002; Williams et al., 2010). Additionally, CN neurons were reported to oscillate in the range of 10–40 Hz in primates performing a precision grip task (Soteropoulos and Baker, 2006; Williams et al., 2010). However, no sign of rhythmic activity was detected in the CN of primates performing wrist and digit movements and natural reaches (Keating and Thach, 1997). Recently, we have shown in freely moving rats that CN neurons display intermittent oscillations in the theta band frequency during repetitive and non-repetitive movements but not during periods of immobility (Baumel and Cohen, 2021).

Essential tremor (ET) is a prevalent motor disorder that causes involuntary, rhythmic tremor, usually in the hands and head (Critchley, 1949, 1972). Tremor is intensified during movements that require accurate control such as pouring water from a bottle or using utensils. These symptoms suggest that the cerebellum, which plays an essential role in the motor control of complex movement, is involved in tremor development (Benito-leon and Labiano-Fontcuberta, 2016). Numerous studies in humans and animals have found evidence implicating the cerebellum with essential tremor (Buijink et al., 2015; Louis et al., 2006; Llinas and Volkind, 1973; Handforth, 2012; Beitz and Saxon, 2004; Welsh, 1998; Weiss and Pellet, 1981; Lamarre and Weiss, 1973; Lamarre et al., 1971; Zhang and Santaniello, 2019; Handforth and Lang, 2021). Harmaline, which is a common animal model of essential tremor, accentuates inferior olivary (IO) subthreshold oscillations, thus increasing the climbing fiber firing rate to about 10 Hz (Llinas et al., 1974; De Montigny and Lamarre, 1973; Pan et al., 2020). This massive complex

* Corresponding author.
E-mail address: danacoh@gmail.com (D. Cohen).

https://doi.org/10.1016/j.heliyon.2021.e08119
Received 2 June 2021; Received in revised form 13 July 2021; Accepted 29 September 2021

spike activity significantly decreases simple spike firing in many Purkinje cells (PCs) while inducing highly synchronized and coherent oscillatory activity (Jacobson et al., 2009; Lamarre et al., 1971; Llinas and Muhlethaler, 1988; Llinas and Volkind, 1973). This altered PC activity propagates to the cerebellar nuclei (CN), which provide the primary output from the cerebellum, where it generates a bursting pattern in the majority of the neurons without altering their firing rate (Brown et al., 2020). Recently, it has been shown that patients with essential tremor, but not healthy control subjects, develop excessive cerebellar oscillations at 10 Hz associated with synaptic pruning deficits of the cerebellar climbing fibers (Pan et al., 2020).

To investigate whether cerebellar oscillations reflect impaired motor output, or alternatively, whether deviations from normal oscillations underlie impaired motor performance we chronically recorded and analyzed neuronal activity in the CN of freely moving rats before and after harmaline treatment. The results show that 57% of the CN neurons oscillated under harmaline, as compared to 28% of the neurons prior to harmaline treatment. In addition, harmaline significantly altered the oscillations' spectral properties, generating incoherent broadband rhythmic activity. These data provide supporting evidence that neuronal oscillations occur in healthy animals and therefore may regularly contribute to motor performance, and that changes in oscillation characteristics may underlie tremor rather than the oscillations themselves.

2. Results

2.1. CN neurons exhibit transient epochs of bursting activity at the theta rhythm in freely moving rats

We recorded 115 well-isolated neurons from the medial (n = 54), the interposed (n = 49) and the lateral cerebellar nuclei (n = 12) of freely moving rats (n = 15). The neurons alternated between diverse firing patterns including prolonged quiescence, stochastic firing and bursting activity as shown in the example neuron in Figure 1A. To capture the diversity in the firing of different CN neurons, we calculated four firing pattern characteristics: the average firing rate, the global and local coefficients of variation (CV and CV2) and the neurons' tendency to release bursts of activity (burst index; see Methods). All of these parameters were broadly distributed (Table 1 and Figures 1B - 1E). The firing rate of single CN neurons ranged from almost complete quiescence (1.7 spikes/s) to an extremely high firing rate of 95.8 spikes/s (31.8 ± 22.2 spikes/s; Figure 1B). The neuronal CV value distribution (2.0 ± 2.6; Figure 1C) suggests that some CN neurons exhibited regular firing (CV < 1), others exhibited random Poisson-like firing (CV ~1), and the remaining neurons alternated between prolonged quiescent periods followed by tonic firing (CV > 1). The CV2 values were also broadly distributed (0.7 ± 0.2; Figure 1D). The burst index (24.8 ± 16%; Figure 1E; see Methods) suggests that some CN neurons hardly ever released bursts, whereas others exhibited mostly bursting activity. The properties of the neurons' bursting activity are summarized in Table 2. A close examination of periods with bursting activity revealed a unique pattern of short bursts on a quiescent background, yielding an On/Off pattern (see an example neuron in Figure 1F). Often this pattern repeated itself and generated a rhythm in the theta range (4–12 Hz frequency band) that occurred intermittently (Figure 1G). This pattern of activity reached significance in 28% (32/115) of the neurons (see Methods). The prevalence of oscillatory neurons was similar across nuclei ($\chi 2$ test; $\chi 2 = 1.94$, $p = 0.38$), henceforth their data were pooled (see Table 1). On average, rhythmic activity took up 46.9 ± 20.9% of the recording time. The dominant frequency was narrowly distributed (7.59 ± 0.89 Hz; Figure 1H), indicating that the vast majority of the neurons oscillated at a

Table 1. Firing characteristics of neurons recorded from different cerebellar nuclei in freely moving control rats.

Nucleus	Firing rate (spikes/s)	CV	CV2	Burst index (%)	% oscillating neurons
	Median (range)	Median (range)	Median (range)	Median (range)	
Medial (n = 54)	32.5 (21.4–56.0)	1.08 (0.78–1.7)	0.59 (0.49–0.78)	20.3 (11.5–32.4)	29.6 (n = 16)
IP (n = 49)	24.3 (13.1–41.1)	1.24 (0.98–1.9)	0.72 (0.56–0.87)	22.9 (11.1–31.5)	22.5 (n = 11)
Lateral (n = 12)	15.2 (7.5–26.3)	1.39 (1.16–2.1)	0.84 (0.73–0.96)	39.2 (22.2–53.8)	41.6 (n = 5)

The range depicts the 25th and 75th percentiles.

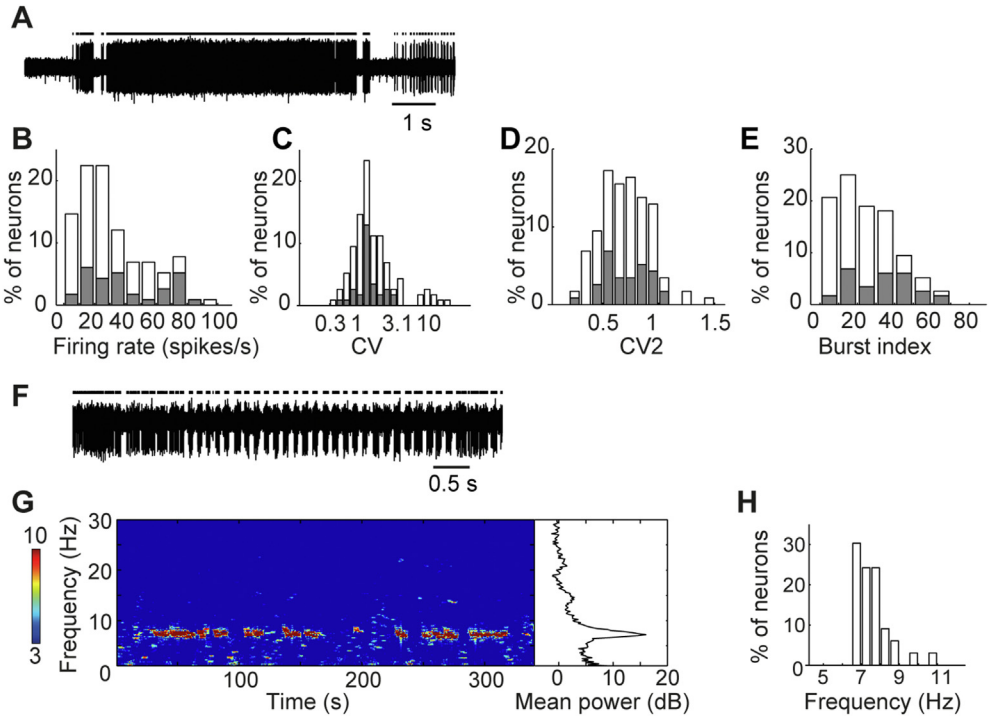

Figure 1. Firing pattern characteristics of CN neurons in freely moving control animals. (A), A representative spike train of a CN neuron exhibiting various firing patterns. Sorted spikes are marked by ticks above the spike train. (B–E), Neuronal population histograms summarizing the firing properties of CN neurons. Shown are firing rate (B), CV (C), CV2 (D), and burst index (E). Non oscillatory neurons are shown in white (n = 83) and oscillatory neurons are shown in gray (n = 32). (F), An example of a CN neuron making a transition from tonic firing to rhythmic bursting activity and back to tonic firing. (G), A spectrogram of the same neuron as in F showing intermittent oscillatory epochs (left). Color bar denotes the spectrogram power in dB. The corresponding average power spectral density (PSD) is shown on the right. (H), The dominant frequency distribution of oscillatory neurons (n = 32).

Table 2. Burst parameters in CN neurons of control and harmaline treated animals.

	Control	Harmaline
	Median (range)	Median (range)
Burst index	23.1 (11.6–35.0) **35.9 (19.0–48.3)**	37.9 (29.5–49.6) **47.9 (37.2–54.2)***
Relative burst duration	16.9 (9.7–24.3) **22.6 (17.4–37.1)**	28.2 (22.1–40.3) **35.4 (25.7–49.8)***
Firing rate within bursts (spikes/s)	133.6 (102.3–170.9) **168.0 (135.6–190.4)**	162.0 (116.4–221.6) **172.9 (125.0–225.6)**
No. of spikes within a burst	4.9 (4.3–5.9) **5 (4.6–5.8)**	4.6 (4.3–5.7) **4.9 (4.4–5.7)**
Burst duration (ms)	49.5 (36.1–67.8) **38.5 (34.5–45.1)**	41.3 (28.4–55.7) **38.7 (27.2–53.3)**

In black are values summarizing the whole population and in bold are values summarizing the oscillatory neurons. The oscillatory neurons displayed significantly different inter-burst properties (Kruskal Wallis; burst index and relative burst duration: $p < 0.001$, marked by * in the table) and similar intra-burst properties (firing rate within bursts, number of spikes within a burst and burst duration; $p > 0.44$) between the control and harmaline conditions. The range depicts the 25th and 75th percentiles.

similar frequency. The bandwidth of the oscillations was relatively narrow: 1.38 ± 0.44 Hz (see Methods), suggesting that regardless of its intermittent nature, the oscillatory process was precise and stable over time.

2.2. Harmaline altered the firing properties of CN neurons

Harmaline induced severe body tremor that became noticeable roughly 3 min post injection and stabilized after about 15 min. We recorded 61 well-isolated neurons from the medial (n = 20), the interposed (n = 33) and the lateral cerebellar nuclei (n = 8) of freely moving rats (n = 12). As in the control animals, we calculated the firing pattern characteristics of neurons under harmaline. During severe body tremor, the average CV, CV2 and burst index of the CN neurons increased significantly as compared to controls (Figure 2B, CV: 2.56 ± 2.08 and 2.0 ± 2.6; Figure 2C, CV2: 0.82 ± 0.17 and 0.7 ± 0.2; and Figure 2D, burst index: 39.7 ± 17% and 24.8 ± 16%; for harmaline and controls, respectively, $p < 0.01$; see Table 3). On average, the firing rate of the CN neurons did not change between the two conditions (Fig. 2A, 31.6 ± 24.3 and 31.8 ± 22.2 spikes/s, for harmaline and controls, respectively; $p = 0.91$). However, examination of 53 CN neurons that were recorded prior to and following harmaline treatment showed that the neurons either increased or decreased their firing rate relative to the controls, reaching significance in 75% (40/53) (paired ttest $p < 0.01$; Figure 2E). Figures 2F-2H shows the CV, CV2 and burst index of these neurons prior to and following harmaline treatment.

The harmaline-induced physiological symptoms were accompanied by the emergence of rhythmic activity in the theta range in a larger fraction of CN neurons than in the controls (harmaline: 57.3% (35/61); χ^2 test; $\chi^2 = 14.76$, $p = 0.0001$). As in controls, the prevalence of oscillatory neurons was similar across nuclei (χ^2 test; $\chi^2 = 0.37$, $p = 0.83$; see Table 3). An example of neuronal spike train and its corresponding spectrogram appear in Figure 2I. The neuron's oscillation frequency was higher and the bandwidth broader under harmaline as compared to the control state. The tendency of a neuron to oscillate under harmaline was independent of whether it oscillated or not in the control condition, and if a neuron oscillated during both conditions its dominant frequency was not necessarily maintained (Figure 2J). As in the controls, under harmaline the oscillatory neurons spanned the entire range of firing property distributions (Figure 2K – 2N; gray bars).

It has been suggested that a regular bursting pattern of activity occurs in the CN neurons of harmaline-treated mice during body tremor (Brown et al., 2020). Our data show that the enhanced rhythmicity in the CN after harmaline treatment was corroborated by increased CV and burst index values, suggesting that CN oscillations may be encoded by bursts as previously reported (Brown et al., 2020). To test whether bursts carry the oscillations, we split each spike train into a time series containing individual spikes and a time series containing spikes that were fired in bursts, and compared their spectral power in the theta band (see Methods). In both the harmaline treated animals and the controls, the bursts' time series exhibited a significantly higher power than the isolated spike time series, thus suggesting that the bursts carried the rhythm in the theta frequency band (Fig. 2O and 2P, paired t-test, $p = 2 \times 10^{-10}$ and $p = 3 \times 10^{-12}$, for the control and harmaline, respectively). Interestingly, while the inter-burst properties of the oscillatory neurons such as the burst index and the relative burst duration changed significantly after harmaline treatment, the intra-burst properties of the oscillatory neurons such as the firing rate within bursts, the number of spikes per burst and the burst durations were similar in the control and under harmaline, suggesting that the process generating bursts was not altered by harmaline (Table 2).

The percent of time spent in oscillations increased significantly in the harmaline treated animals as compared to the controls (Fig. 2Q, control: 46.9 ± 20.9%; harmaline: 64.5 ± 24.0%; $p < 0.005$). In addition, the range of the oscillations' dominant frequency was broad and the average frequency increased significantly under harmaline as compared to the controls (Fig. 2R, control: 7.59 ± 0.89 Hz; harmaline: 8.53 ± 2.31 Hz; $p < 0.005$). The broadening of the dominant frequency distribution was not the outcome of variability in the harmaline concentration because simultaneously recorded neurons exhibited different dominant frequencies (Figure 2S). In addition, the bandwidth around the dominant peak widened significantly (control: 1.38 ± 0.44 Hz; harmaline: 2.88 ± 1.24 Hz; $p < 0.01$; Fig. 2T). These data indicate that despite the harmaline-induced increase in rhythmicity, the spectral features of the neurons reflected a less organized, inaccurate oscillatory process.

2.3. Neuronal coherence and the coordination of oscillatory epochs were substantially reduced under harmaline

To better understand the impact of oscillations on CN computation, we tested whether the detected oscillation epochs occurred simultaneously or sporadically in simultaneously recorded neurons in the controls and under harmaline. Figure 3A shows a pair of CN neurons recorded simultaneously from a freely moving control rat that co-oscillated throughout the recording time despite the intermittent nature of the oscillations. To quantify the likelihood of pairs of simultaneously recorded neurons to co-oscillate, we measured the probability of co-occurring oscillatory bins in all the simultaneously recorded neuronal pairs (n = 23) and compared this to the probability calculated when assuming independent oscillatory processes in the different neurons. The measured probability of co-occurring oscillatory bins in simultaneously recorded neurons was significantly higher than the expected probability, indicating that the oscillatory epochs were better timed than the randomly occurring oscillations (Figure 3C; observed probability: 36.3 ± 11.8%; expected probability: 22.5 ± 10.4%; paired t-test; $p < 0.001$).

We then investigated how harmaline influenced the likelihood of pairs of simultaneously recorded neurons to co-oscillate. Figure 3B depicts an example of two simultaneously recorded neurons that oscillated at the same frequency, but at different times. Under harmaline, the measured probability of co-occurring oscillatory epochs was similar to that expected from randomly occurring oscillations (n = 36 pairs; Figure 3D; observed probability: 47.9 ± 19%; expected probability: 46.74 ± 19.1%; paired t-test; $p = 0.79$).

We then investigated whether simultaneously recorded pairs of neurons tended to oscillate at a similar frequency. Figure 3E demonstrates in the controls that the majority of the oscillatory bins of simultaneously recorded pairs of neurons oscillated at the same frequency throughout the recordings (mean frequency deviation: 0.52 ± 0.35 Hz). In contrast, Figure 3F demonstrates that under harmaline for most of the

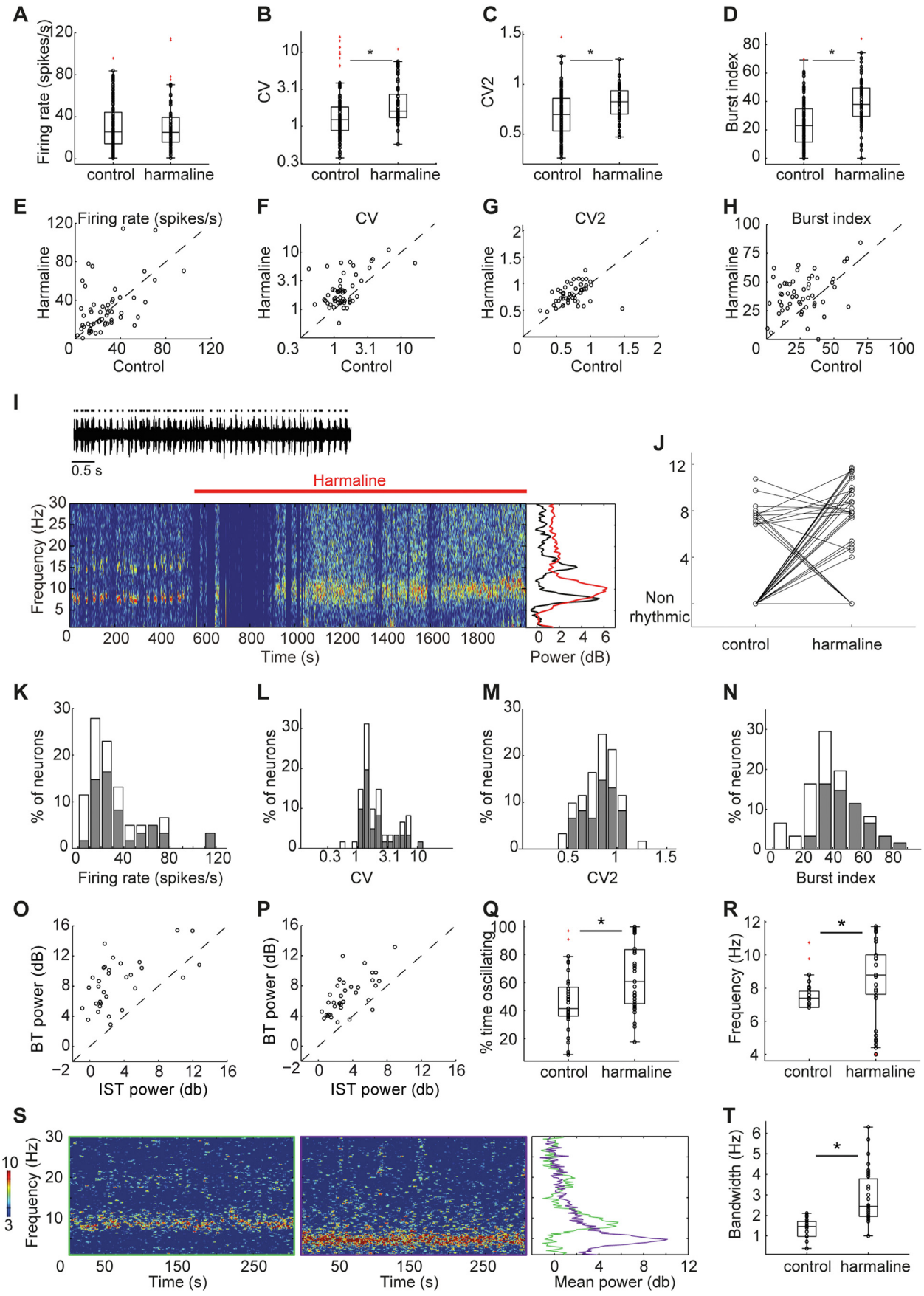

(caption on next page)

Table 3. Firing characteristics of neurons recorded from different cerebellar nuclei in harmaline treated rats.

Nucleus	Firing rate (spikes/s)	CV	CV2	Burst index (%)	% oscillating neurons
	Median (range)	Median (range)	Median (range)	Median (range)	
Medial (n = 20)	29.8 (20.9–57.2)	1.47 (1.3–2.2)	0.81 (0.68–0.90)	36.8 (28.7–46.8)	55 (n = 11)
IP (n = 33)	19.5 (13.0–33.1)	2.0 (1.43–4.78)	0.84 (0.72–0.95)	39.1 (29.9–52.4)	57.6 (n = 20)
Lateral (n = 8)	20.8 (10.5–26.9)	1.29 (1.24–2.0)	0.99 (0.88–1.1)	46.8 (30.8–53.8)	62.5 (n = 4)

The range depicts the 25th and 75th percentiles.

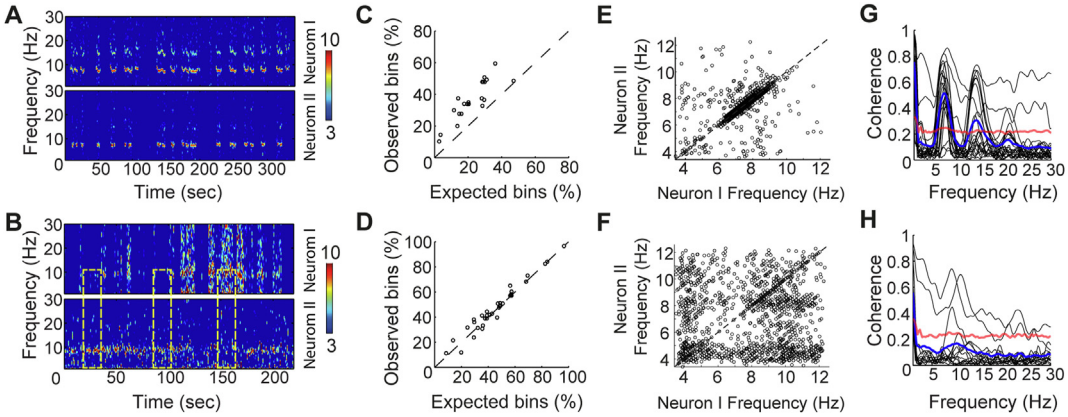

Figure 3. Fewer well-coordinated highly coherent oscillatory epochs observed under harmaline as compared to controls. (A), An example of two co-oscillating CN neurons recorded from control animals. (B), An example of two simultaneously recorded neurons that oscillated at the same frequency but at different times under harmaline. Yellow dotted rectangles depict times at which one neuron oscillated while the other did not. (C), The expected (abscissa) vs. the observed (ordinate) co-oscillating bins in the control animals (n = 32). The diagonal dotted line indicates equal values. (D), Same as (C) for harmaline (n = 35). (E), For each pair of simultaneously recorded neurons, fifty 5 s bins of co-oscillations were randomly selected and the dominant frequencies of both neurons were plotted against each other (n = 23 pairs, 50 bins per pair, see Methods). (F), Same as (E) for harmaline (n = 36 pairs, 50 bins per pair). (G), Neuronal pairwise cross-coherence calculated for all co-oscillating bins within a neuronal pair in the controls (n = 23). Thick blue line is the coherence averaged across all pairs. The red line marks the average 99th percentile confidence level. (H), Same as (G) for harmaline (n = 15).

recording time, simultaneously recorded neuronal pairs oscillated at different frequencies (mean frequency deviation: 2.86 ± 1.53 Hz; see example in Figure 2S for 2 simultaneously recorded neurons that oscillated at different frequencies).

Next we tested whether simultaneously recorded neurons that oscillated at the same frequency also maintained a constant phase lag, by calculating their coherence in the theta band frequency. The findings showed that 87% (20/23) of the oscillatory neuronal pairs exhibited a significantly high coherence when recorded in the controls (Figure 3G, bootstrap; $p < 0.01$, see Methods). Hence despite the fact that the oscillatory activity was intermittent, it was well-timed and maintained the same frequency and phase throughout the session (Figure 3, top row). Interestingly, 6 out of 8 (75%) neuronal pairs that were recorded from different hemispheres also exhibited significant coherence.

Repetition of this analysis in harmaline treated animals revealed a completely different scenario. Only 42 % (15/36) of the simultaneously recorded pairs of neurons that oscillated at the same time oscillated at the same dominant frequency. Of these, only 20% (3/15) exhibited significantly high coherence (Figure 3H, bootstrap; $p < 0.01$). Thus, in harmaline treated animals, the induced oscillations tended not to occur at the same time in simultaneously recorded pairs of neurons, the oscillations could occur at different frequencies, and those neurons that oscillated at the same frequency did not maintain a stable phase, thus resulting in reduced coherence (Figure 3, bottom row).

Figure 2. Firing pattern characteristics in freely moving animals following systemic harmaline treatment. (A–D), Population firing characteristics in the control and harmaline conditions for firing rate (A), CV (B), CV2 (C), and burst index (D). Boxplots denote the population medians with the edges at the 25th and 75th percentiles. Vertical lines denote the 5th and the 95th percentiles. Each neuron is represented by a black circle and a red plus sign marks outliers. Black asterisks denote a significant difference between groups ($p < 0.01$). (E–H), Firing pattern characteristics of neurons that were recorded before (abscissa) and after (ordinate) harmaline injection (n = 53). The diagonal dashed line marks equal values. Shown are firing rates (E), CV (F), CV2 (G) and burst index (H). (I), An example of a CN neuron spike train after harmaline injection (top) and its spectrogram (bottom, left), showing robust oscillatory activity. Color bar denotes the spectrogram power in dB. The corresponding PSD is shown on the right for control (black) and after harmaline injection (red). (J), The observed dominant frequency band of each neuron before and after harmaline injection. (K–N), Neuronal population histograms summarizing the firing properties of CN neurons under harmaline. Shown are firing rate (K), CV (L), CV2 (M), and burst index (N). Non oscillatory neurons are shown in white (n = 26) and oscillatory neurons are shown in gray (n = 35). (O), The dominant frequency power of the bursts-only spike train PSD (ordinate) was significantly higher than the power of the isolated spike train PSD (abscissa). The diagonal dotted line indicates equal values. (P), The same as in (O) for harmaline. (Q–R), Shown are the relative oscillation time (Q) and the dominant oscillation frequency (R) for neurons in the control (n = 32) and harmaline treated animals (n = 35). Boxplots depict the population medians with the edges at the 25th and 75th percentiles. Vertical lines mark the 5th and the 95th percentiles and a red plus sign marks outliers. Black asterisks denote a significant difference between groups ($p < 0.01$). (S), Shown is an example of two neurons recorded simultaneously under harmaline in which one neuron oscillated at 9.5 Hz (left, green) whereas the other neuron oscillated at 4.2 Hz (right, purple). Color bar denotes the spectrogram power in dB. The mean power spectral densities of the two neurons are shown on the right. This phenomenon occurred in 21/36 (58 %) of the simultaneously recorded neuronal pairs under harmaline. (T), Shown is the oscillation bandwidth for neurons in the control (n = 32) and harmaline treated animals (n = 35). Boxplots depict the population medians with the edges at the 25th and 75th percentiles. Vertical lines mark the 5th and the 95th percentiles and a red plus sign marks outliers. Black asterisks denote a significant difference between groups ($p < 0.01$).

The significant differences between oscillation characteristics measured in controls and under harmaline suggest that the impaired rhythmic process may be a primary factor influencing the emergence of body tremor rather than the mere existence of oscillations.

3. Discussion

In the current study we recorded the activity of CN neurons in freely moving rats and after harmaline treatment. In both conditions, CN neurons exhibited oscillatory activity in the theta range, but the fraction of oscillatory neurons under harmaline was almost twice that of the controls. In freely moving rats, the CN neurons exhibited well-timed, highly coherent rhythmic bursting activity at 7–8 Hz whereas under harmaline, concomitantly to the generation of body tremor, neuronal oscillations occurred randomly at different frequencies and impaired coherence. Taken together, these data suggest that the occurrence of oscillations per se is not likely to underlie emergent body tremor. We thus posit that abnormal CN computation expressed in the substantial increase in the number of oscillatory neurons, the occurrence of multiple dominant frequencies, the loss of coherence, the reduced oscillation precision and the impaired coordination of transient oscillatory epochs may all or singly underlie the emergence of body tremor.

We showed that in freely moving rats about 30% of CN neurons exhibited well-timed, highly coherent rhythmic bursting activity at 7–8 Hz. The source of this rhythmic activity remains unclear. It has been suggested that the principles of the olivo-cerebellar network point more strongly toward a role for synchrony based, dynamic spatiotemporal patterning in cerebellar processing (De Zeeuw et al., 2011). Moreover, cerebellar nuclear neurons are preferentially tuned to the spike timing of synchronized Purkinje cells and may therefore amplify IO generated synchrony (Sugihara et al., 1993; Handforth and Lang, 2021). However, other sources of rhythmic patterns cannot be excluded. The primary somatosensory cortex has been shown to strongly influence CN activity via the mossy fibers (Rowland et al., 2010). Nevertheless, while coherent slow wave oscillations (~1 Hz) were reliably conveyed through the cerebrocerebellar loop, gamma band activity was not (Schwarz, 2009) thus hinting that the CN may actively filter specific frequencies. Interestingly, the granular cells, which are excited by mossy fibers and in turn excite the PCs, were found to show a resonance frequency in the range of 6–14 Hz (D'Angelo et al., 2009) which may indicate a preferred frequency carried by the mossy fibers.

The CN contain a bilateral movement representation and show relatively direct, powerful access to limb muscles on both sides of the body, which puts the cerebellum in an ideal position to coordinate bilateral movements (Soteropoulos and Baker, 2008). In fact, anatomical connectivity enabling complex spike synchronization between the left and right cerebellar hemispheres has been described (De Zeeuw et al., 1996). This property of the cerebellar cortex may be transferred to the CN, thus accounting for the high coherence observed between pairs of CN neurons recorded bilaterally in freely moving animals.

Harmaline induces network oscillations at about 10 Hz, originating in the IO and spreading into the cerebellar cortex and the CN (Milner et al., 1995; Llinas and Volkind, 1973; Park et al., 2010). We showed that most neuronal pairs in the CN oscillate at different dominant frequencies, and even those that oscillated at the same frequency did not maintain a constant phase, suggesting that under harmaline other factors may influence CN activity. Systemic application of harmaline may influence a variety of intrinsic CN neuronal properties, for example, via serotonin overflow which differentially influences CN neuronal activity and modulates its synaptic efficacy (Di Mauro et al., 2003; Saitow et al., 2009; Murano et al., 2011), and/or extrinsically alter CN afferents by enhancing rhythmicity in the climbing fibers, promoting complex spike activity over the stochastic simple spike activity in PCs, and inducing abnormal feedback from the mossy fibers. Importantly, the mossy fiber inputs are attenuated by increased levels of serotonin (Murano et al., 2011) which may hint at their more negligible influence under systemic harmaline application.

In the human disease of ET the occurrence of abnormal activity and structural changes in the IO remain controversial (Louis and Lenka, 2017). By contrast, structural changes in the cerebellum, particularly in the PCs, have been described both in human patients (Babij et al., 2013; Louis et al., 2013a, 2013b, 2014) and in rodents following harmaline treatment at high dosages (Miwa et al., 2006, O'Hearn and Molliver, 1993). It remains to be discovered whether neuronal activity in the CN of ET patients has similar spectral characteristics during tremor as described here.

The harmaline-induced body tremor depends on intact olivocerebellar connectivity (Llinas and Volkind, 1973). Mutant mice lacking gap junctions in the IO show uncorrelated pairwise neuronal activity, whereas neighboring pairs of wild-type olivary neurons are strongly synchronized (Long et al., 2002). Nevertheless, the mutant mice develop pronounced tremor when exposed to harmaline, identical to wild-type mice (Kistler et al., 2002; Long et al., 2002). While it has been suggested that the sparing of tremor in the absence of gap junctions can be attributed to developmental compensation in olivary neurons (De Zeeuw et al., 2003), we put forward an alternative but complementary interpretation: the lack of olivary synchrony contributes to the already a-synchronous activity in the CN so that tremor occurs in both wild type and mutant mice. In the unlesioned animal, cooling of the cerebellar cortex was reported to produce desynchronization of rhythmic motoneuron firing without eliminating the tremor (Llinas and Volkind, 1973). Only lesions of the olivo-cerebellar pathway (Park et al., 2010; Llinas and Volkind, 1973) or blocking the Purkinje cells' input to the CN (Brown et al., 2020) caused the tremor to cease, thus lending additional weight to the claim that IO afferents supply the basic rhythm and that any source of desynchronization, rather than eliminating the tremor, enhances the incoherent activity already present in the CN, thus sparing body tremor.

Tremor is caused by unintentional and uncontrollable rhythmic movement of the body, thus raising the question how could disruption of an accurate spectral structure cause tremor? A plausible explanation comes from studies in non-human primates performing slow finger movements (Williams et al., 2009, 2010). During these movements, neurons in the CN, the primary motor cortex and the spinal cord displayed coherent rhythmic activity, but, the spinal cord neurons were approximately 180° phase lagged relative to both the CN and the primary motor cortex. The authors posit that convergence of antiphase oscillations from these structures and others in the motor production network would lead to cancellation of natural oscillations at the motoneuronal level, thereby reducing tremor and improving movement precision (Williams et al., 2010). We suggest that the aberrant spectral structure in the CN following harmaline treatment prevents the cancellation of the natural oscillations in the motoneurons, thus generating action tremor.

We showed the occurrence of oscillations in freely moving normal rats, thus suggesting that oscillations per se are not likely to cause tremor. In the harmaline model of essential tremor, in addition to the enhanced number of oscillatory neurons and the lengthening of oscillation time, the accuracy of the spectral structure breaks down. Taken together, we suggest that in normal animals, the CN may extract and amplify short lasting oscillations concealed within PC ensembles (Person and Raman, 2012; Yarom and Cohen, 2002), thus producing the observed transient oscillations (Baumel and Cohen, 2021). In harmaline treated animals, CN neurons are bombarded with strong rhythmic input from the Purkinje cells (Jacobson et al., 2009; Brown et al., 2020) which likely causes them to be shifted out of their dynamic range; thus, instead of extracting PC rhythm reliably, the CN neurons exhibit abnormal rhythm.

4. Materials and methods

All procedures were approved by the Bar Ilan University Institutional Animal Care and Use Committee and were performed in accordance with the National Institutes of Health guidelines. During the experiments, the

animals were housed in individually ventilated cages with a metal compartment allowing odor exchange between two sides of the cage (Tecniplast). Food and water were available *ad libitum*, in a room with a 12 h light/dark cycle.

4.1. Surgery

The surgical procedures have been described elsewhere in detail (Jacobson et al., 2009; Baumel et al., 2009). In brief, 15 adult Long Evans male rats weighing 350–500 g (Harlan, Indianapolis, IN, USA) were initially sedated with 5% isoflurane and then injected intramuscularly with ketamine HCl and xylazine HCl (100 and 10 mg/kg, respectively). Supplementary injections of ketamine and xylazine were given as required. The skull surface was exposed and 1 or 2 craniotomies, slightly larger than the implanted electrodes, were made above the medial (AP: -11, ML: ±1; n = 6 rats), interposed (AP: -11, ML: ±1.5; n = 5 rats), or lateral (AP: -11.5, ML: ±3.5; inserted at 20° angle; n = 4 rats) nuclei (Paxinos and Watson, 1998). 16 microwires (35 μm, isonel coated tungsten; California Fine Wire Company) arranged in 4 × 4 arrays or 16 microwires (25 μm, formvar coated nichrom; A-M Systems, Inc.) inserted into a 29 gauge cannula were lowered 3.4–4.5 mm from the surface of the brain and fixed using dental cement. Postoperative care included Carprofen administration (5 mg/kg; subcutaneous) at 24 and 48 h post-surgery. The animal's state was evaluated based on predefined parameters and additional injections were given accordingly. Rats were given ≥1 week to recover prior to recording. Electrode location was verified histologically after performing electrolytic lesions, perfusion with 4% formalin, brain fixation with 20% sucrose-formalin and cryostat 50 μm thick sectioning.

4.2. Data acquisition

Neural activity was amplified, band-pass filtered at 150–8000 Hz and sampled at 40 kHz using a multichannel acquisition processor system (MAP system; Plexon Inc.). Activity was recorded for 15 min in freely moving animals. In sessions where multiple single units were recorded, the animal was lightly sedated (5% isoflurane) and then injected intraperitoneally with harmaline HCl (10–15 mg/kg; Sigma-Aldrich). Neuronal activity was recorded for 15 min after the harmaline-induced body tremor stabilized (~10–20 min). Offline sorting (offline sorter, Plexon Inc.) was performed on all recorded channels containing units with a signal to noise ratio of more than 3:1. A unit was considered a single neuron if its waveform generated a distinct cluster in the principal component analysis performed by the software. Only single neurons were included for further analysis in MATLAB (R2013b, MathWorks Inc., Natick, MA).

4.3. Data analyses

Firing rate. was calculated as the total number of spikes divided by the duration of the recording session.

CV. is the coefficient of variation defined as the standard deviation of the interspike interval (ISI) distribution divided by its mean.

CV2. is defined as the difference between two consecutive ISIs divided by their mean.

Burst detection. The probability of encountering an ISI of length x or shorter, given the preceding interval, was calculated using a measure of the instantaneous discharge probability (Pauluis and Baker, 2000) based on the cumulative gamma distribution.

$$p(x \mid A, isi_{(i)}) = \frac{1}{A^{isi_{(i)}+1}} \int_0^x t \cdot e^{\frac{-t}{isi_{(i)}}}\, dt$$

Burst initiation was said to occur if two consecutive intervals were shorter than the median ISI and the probability of finding intervals of that duration was < 0.05 based on a gamma distribution whose average ISI was equal to the preceding reference interval. The gamma distribution shape parameter, A = 2, was chosen based on its best fit to the dataset. Burst termination was determined according to the Poisson surprise method (Legendy and Salcman, 1985; Benhamou et al., 2012).

Burst index was defined as the number of spikes occurring within bursts divided by the total number of spikes.

Relative burst duration was defined as the sum of all burst durations divided by the total recording time.

Number of spikes within a burst was defined as the sum of spikes in all bursts divided by the number of bursts.

Burst duration was defined as the sum of all burst durations divided by the number of bursts.

Firing rate within a burst was defined as the number of spikes divided by burst duration and averaged across all bursts.

Power spectrum. For each spike train, an autocorrelation was computed in 5 s bins with a 50% overlap and transformed into the spectral domain using the Fast Fourier Transform. The power was normalized to dB. A neuron was considered oscillatory if its peak exceeded the 95% confidence interval of the χ^2 distribution of the mean power in the 30–50 Hz band and was > 3 dB above the power in adjacent frequency bins to prevent the inclusion of noisy bins with large power variation in all frequencies (Percival and Walden, 1993). The same criteria were used for detecting oscillatory bins. The bandwidth of the oscillatory process was defined as the width of the power spectral density peak at half amplitude.

The expected probability of co-occurring oscillatory bins. The probability of each neuron to oscillate was defined as the fraction of oscillatory bins out of the whole recording. The expected probability of two neurons to co-oscillate assuming independent processes was calculated as the product of the probability of each neuron to oscillate.

Coherence. Coherence was calculated by dividing the square of the absolute value of the cross spectrum by the product of the power spectrum of the two neurons. Coherence was computed for time bins in which significant power was obtained in both neurons. The significance of pairwise coherence was assessed independently for each pair of simultaneously recorded neurons by calculating confidence intervals using a bootstrap technique. Specifically, the pairwise coherence was recalculated after randomly assigning a phase difference for each bin in which both neurons oscillated. Confidence intervals were calculated from the distribution of 200 repetitions over the artificially calculated coherence values. If the coherence value exceeded the confidence intervals set at p < 0.01, the coherence between the pair of neurons was considered significant.

Statistics. All the data are presented as mean ± SD unless otherwise specified. The Kruskal-Wallis test for non-parametric distributions was used to statistically compare data between the two experimental control and harmaline conditions, unless otherwise specified. A χ2 test of occurrence was used to test for significance of oscillation co-occurrence and the fraction of oscillatory neurons.

Declaration

Author contribution statement

Yuval Baumel: Conceived and designed the experiments; Performed the experiments; Analyzed and interpreted the data; Wrote the paper.

Hagar G. Yamin: Analyzed and interpreted the data; Wrote the paper.

Dana Cohen: Conceived and designed the experiments; Analyzed and interpreted the data; Wrote the paper.

Funding statement

This research was supported by a REALNET grant from the European Commission (FP7-ICT270434) and by SYNCH project funded by the

European Commission under H2020 FET Proactive programme (Grant agreement ID: 824162).

Data availability statement

Data will be made available on request.

Declaration of interests statement

The authors declare no conflict of interest.

Additional information

No additional information is available for this paper.

References

Babij, R., Lee, M., Cortes, E., Vonsattel, J.P., Faust, P.L., Louis, E.D., 2013. Purkinje cell axonal anatomy: quantifying morphometric changes in essential tremor versus control brains. Brain 136, 3051–3061.

Baumel, Y., Cohen, D., 2021. State-dependent entrainment of cerebellar nuclear neurons to the local field potential during voluntary movements. J. Neurophysiol. 126, 112–122.

Baumel, Y., Jacobson, G.A., Cohen, D., 2009. Implications of functional anatomy on information processing in the deep cerebellar nuclei. Front. Cell. Neurosci. 3, 14.

Beitz, A.J., Saxon, D., 2004. Harmaline-induced climbing fiber activation causes amino acid and peptide release in the rodent cerebellar cortex and a unique temporal pattern of Fos expression in the olivo-cerebellar pathway. J. Neurocytol. 33, 49–74.

Benhamou, L., Bronfeld, M., Bar-Gad, L., Cohen, D., 2012. Globus pallidus external segment neuron classification in freely moving rats: a comparison to primates. PLoS One 7, e45421.

Benito-leon, J., Labiano-Fontcuberta, A., 2016. Linking essential tremor to the cerebellum: clinical evidence. Cerebellum 15, 253–262.

Brown, A.M., White, J.J., van der Heijden, M.E., Zhou, J., Lin, T., Sillitoe, R.V., 2020. Purkinje cell misfiring generates high-amplitude action tremors that are corrected by cerebellar deep brain stimulation. Elife 9.

Brown, P., 2006. Bad oscillations in Parkinson's disease. J. Neural. Transm. Suppl, 27–30.

Buijink, A.W., Broersma, M., van der Stouwe, A.M., van Wingen, G.A., Groot, P.F., Speelman, J.D., Maurits, N.M., Van Rootselaar, A.F., 2015. Rhythmic finger tapping reveals cerebellar dysfunction in essential tremor. Park. Relat. Disord. 21, 383–388.

Buschman, T.J., Miller, E.K., 2009. Serial, covert shifts of attention during visual search are reflected by the frontal eye fields and correlated with population oscillations. Neuron 63, 386–396.

Buzsaki, G., 2006. Rhythms of the Brain. Oxford University Press.

Conway, B.A., Halliday, D.M., farmer, S.F., Shahani, U., Maas, P., Weir, A.I., Rosenberg, J.R., 1995. Synchronization between motor cortex and spinal motoneuronal pool during the performance of a maintained motor task in man. J. Physiol. 489 (Pt 3), 917–924.

Courtemanche, R., Pellerin, J.-P., Lamarre, Y., 2002. Local field potential oscillations in primate cerebellar cortex: modulation during active and passive expectancy. J. Neurophysiol. 88, 771–782.

Courtemanche, R., Robinson, J.C., Aponte, D.I., 2013. Linking oscillations in cerebellar circuits. Front. Neural Circ. 7, 125.

Critchley, E., 1972. Clinical manifestations of essential tremor. J. Neurol. Neurosurg. Psychiatry 35, 365–372.

Critchley, M., 1949. Observations on essential (heredofamial) tremor. Brain 72, 113–139.

D'Angelo, E., Koekkoek, S.K., Lombardo, P., Solinas, S., Ros, E., Garrido, J., Schonewille, M., de Zeeuw, C.I., 2009. Timing in the cerebellum: oscillations and resonance in the granular layer. Neuroscience 162, 805–815.

De Montigny, C., Lamarre, Y., 1973. Rhythmic activity induced by harmaline in the olivo-cerebello-bulbar system of the cat. Brain Res. 53, 81–95.

De Zeeuw, C.L., Chorev, E., Devor, A., Manor, Y., Van der Giessen, R.S., de Jeu, M.T., Hoogenraad, C.C., Bijman, J., Ruigrok, T.J.H., French, P., Jaarsma, D., Kistler, W.M., Meier, C., Petrasch-Parwez, E., Dermietzel, R., Sohl, G., Gueldenagel, M., Willecke, K., Yarom, Y., 2003. Deformation of network connectivity in the inferior olive of connexin 36-deficient mice is compensated by morphological and electrophysiological changes at the single neuron level. J. Neurosci. 23, 4700–4711.

De Zeeuw, C.L., Hoebeek, F.E., Bosman, L.W., Schonewille, M., Witter, l., Koekkoek, S.K., 2011. Spatiotemporal firing patterns in the cerebellum. Nat. Rev. Neurosci. 12, 327–344.

De Zeeuw, c.I., lang, e.J., sugihara, i., ruigrok, t.J.H., eisenman, l.M., mugnaini, e., llinas, r., 1996. Morphological correlates of bilateral synchrony in the rat cerebellar cortex. J. Neurosci. 16, 3412–3426.

Di Mauro, m., Fretto, g., Caldera, m., Li volsi, g., Licata, f., Ciranna, l., Santangelo, f., 2003. Noradrenaline and 5-hydroxytryptamine in cerebellar nuclei of the rat: functional effects on neuronal firing. Neurosci. Lett. 347, 101–105.

Donoghue, J.P., Sanes, J.N., Hatsopoulos, N.G., Gaal, G., 1998. Neural discharge and local field potential oscillations in primate motor cortex during voluntary movements. J. Neurophysiol. 79, 159–173.

Gross, J., timmermann, l., Kujala, J., Dirks, M., Schmitz, F., Salmelin, R., Schnitzler, A., 2002. The neural basis of intermittent motor control in humans. Proc. Natl. Acad. Sci. U. S. A. 99, 2299–2302.

Handforth, A., 2012. Harmaline tremor: underlying mechanisms in a potential animal model of essential tremor. Tremor. Other Hyper. Mov (N Y) 2.

Handforth, A., Lang, E.J., 2021. Increased purkinje cell complex spike and deep cerebellar nucleus synchrony as a potential basis for syndromic essential tremor. A review and synthesis of the literature. Cerebellum 20, 266–281.

Jacobson, G.A., Lev, I., Yarom, Y., Cohen, d., 2009. Invariant phase structure of olivo-cerebellar oscillations and its putative role in temporal pattern generation. Proc. Natl. Acad. Sci. U. S. A. 106, 3579–3584.

Kayser, C., Montemurro, M.A., logothetis, n.K., panzeri, s., 2009. Spike-phase coding boosts and stabilizes information carried by spatial and temporal spike patterns. Neuron 61, 597–608.

Keating, J.G., Thach, W.T., 1997. No clock signal in the discharge of neurons in the deep cerebellar nuclei. J. Neurophysiol. 77, 2232–2234.

Kiehn, O., Kjaerulff, O., 1998. Distribution of central pattern generators for rhythmic motor outputs in the spinal cord of limbed vertebrates. Ann. N. Y. Acad. Sci. 860, 110–129.

Kistler, W.M., De Jeu, M.T.G., Elegersma, Y., van der giessen, R.S., Hensbroek, R., Lou, C., Koekkoek, S.K.E., Hoogenradd, C.C., Hamers, F.P.T., Gueldenagel, M., Sohl, G., Willecke, K., de Zeeuw, C.I., 2002. Analysis of Cx36 knockout does not support tenet that olivary gap junctions are required for complex spike synchronization and normal motor performance. Ann. NY Acad. Sci. 978, 391–404.

Kondylis, E.D., Randazzo, M.J., Alhourani, A., Lipski, W.J., Wozny, T.A., Pandya, Y., Ghuman, A.S., Turner, R.S., Crammond, D.J., Richardson, R.M., 2016. Movement-related dynamics of cortical oscillations in Parkinson's disease and essential tremor. Brain 139, 2211–2223.

Lamarre, Y., de Montigny, C., Dumont, M., Weiss, M., 1971. Harmaline-induced rhythmic activity of cerebellar and lower brain stem neurons. Brain Res. 32, 246–250.

Lamarre, Y., Weiss, M., 1973. Harmaline-induced rhythmic acitivity of alpha and gamma motoneurons in the cat. Brain Res. 63, 430–434.

Legendy, C.R., Salcman, M., 1985. Bursts and recurrences of bursts in the spike trains of spontaneously active striate cortex neurons. J. Neurophysiol. 53, 926–939.

Levesque, M., Gao, H., Southward, C., Langlois, J.M.P., Lena, C., Courtemanche, R., 2020. Cerebellar cortex 4-12 Hz oscillations and unit phase relation in the awake rat. Front. Syst. Neurosci. 14, 475948.

Llinas, R., Baker, R., Sotelo, C., 1974. Electrotonic coupling between neurons in cat inferior olive. J. Neurophysiol. 37, 560–571.

Llinas, R., Muhlethaler, M., 1988. Electrophysiology of Guinea-pig cerebellar nuclear cells in the in vitro brain stem-cerebellar preparation. J. Physiol. 404, 241–258.

Llinas, R., Volkind, R.A., 1973. The olivo-cerebellar system: functional properties as revealed by harmaline-induced tremor. Exp. Brain Res. 18, 69–87.

Long, M.A., Deans, M.R., Paul, D.L., Connors, B.W., 2002. Rhythmicity without synchrony in the electrically uncoupled inferior olive. J. Neurosci. 22, 10898–10905.

Louis, E.D., Babij, R., Cortes, E., vonsattel, J.P., Faust, P.L., 2013a. The inferior olivary nucleus: a postmortem study of essential tremor cases versus controls. Mov. Disord. 28, 779–786.

Louis, E.D., Babij, R., Lee, M., Cortes, E., Vonsattel, J.P., 2013b. Quantification of cerebellar hemispheric purkinje cell linear density: 32 ET cases versus 16 controls. Mov. Disord. 28, 1854–1859.

Louis, E.D., Lee, M., Babij, R., Ma, K., Cortes, E., Vonsattel, J.P., Faust, P.L., 2014. Reduced Purkinje cell dendritic arborization and loss of dendritic spines in essential tremor. Brain 137, 3142–3148.

Louis, E.D., Lenka, A., 2017. The olivary hypothesis of essential tremor: time to lay this model to rest? Tremor. Other Hyper. Mov. (N Y) 7, 473.

Louis, E.D., vonsattel, J.P., Honig, l.S., Lawton, A., Moskowitz, C., Ford, B., Frucht, S., 2006. Essential tremor associated with pathologic changes in the cerebellum. Arch. Neurol. 63, 1189–1193.

Mallet, N., Pogosyan, A., Sharott, A., Csicsvari, J., Bolam, J.P., Brown, P., Magill, P.J., 2008. Disrupted dopamine transmission and the emergence of exaggerated beta oscillations in subthalamic nucleus and cerebral cortex. J. Neurosci. 28, 4795–4806.

Mazzoni, A., Panzeri, S., Logothetis, N.K., Brunel, n., 2008. Encoding of naturalistic stimuli by local field potential spectra in networks of excitatory and inhibitory neurons. PLoS Comput. Biol. 4, e1000239.

Milner, T.E., Cadoret, G., Lessard, l., Smith, A.M., 1995. EMG analysis of harmaline-induced tremor in normal and three strains of mutant mice with Purkinje cell degeneration and the role of the inferior olive. J. Neurophysiol. 73, 2568–2577.

Miwa, H., Kubo, T., Suzuki, A., Kihira, T., Kondo, T., 2006. A species-specific difference in the effects of harmaline on the rodent olivocerebellar system. Brain Res. 1068, 94–101.

Murano, M., saitow, f., suzuki, h., 2011. Modulatory effects of serotonin on glutamatergic synaptic transmission and long-term depression in the deep cerebellar nuclei. Neuroscience 172, 118–128.

Muthuraman, M., Heute, U., Arning, K., Anwar, A.R., Elble, R., Deuschl, G., Raethjen, J., 2012. Oscillating central motor networks in pathological tremors and voluntary movements. What makes the difference? Neuroimage 60, 1331–1339.

O'Hearn, E., Molliver, M.E., 1993. Degeneration of Purkinje cells in parasagittal zones of the cerebellar vermis after treatment with ibogaine or harmaline. Neuroscience 55, 303–310.

Pan, M.K., Li, Y.S., Wong, S.B., Ni, C.L., Wang, Y.M., Liu, W.C., Lu, l.Y., Lee, J.C., Cortes, E.P., Vonsattel, J.G., Sun, Q., Louis, E.D., Faust, P.L., Kuo, S.H., 2020. Cerebellar oscillations driven by synaptic pruning deficits of cerebellar climbing fibers contribute to tremor pathophysiology. Sci. Transl. Med. 12.

Park, Y.G., Park, H.Y., Lee, C.J., Choi, S., Jo, S., Choi, H., Kim, Y.H., Shin, H.S., llinas, R.R., Kim, D., 2010. Ca(V)3.1 is a tremor rhythm pacemaker in the inferior olive. Proc. Natl. Acad. Sci. U. S. A. 107, 10731–10736.

Pauluis, Q., Baker, S.N., 2000. An accurate measure of the instantaneous discharge probability, with application to unitary joint-event analysis. Neural Comput. 12, 647–669.
Paxinos, G., Watson, C., 1998. The Rat Brain in Stereotaxic Coordinates. Academic Press, San Diego.
Percival, D.B., Walden, A.T., 1993. Spectral Analysis for Physical Applications. Cambridge University Press.
Person, A.L., Raman, I.M., 2012. Purkinje neuron synchrony elicits time-locked spiking in the cerebellar nuclei. Nature 481, 502–505.
Pinault, D., Vergnes, M., Marescaux, C., 2001. Medium-voltage 5-9-Hz oscillations give rise to spike-and-wave discharges in a genetic model of absence epilepsy: in vivo dual extracellular recording of thalamic relay and reticular neurons. Neuroscience 105, 181–201.
Ribary, U., 2005. Dynamics of thalamo-cortical network oscillations and human perception. Prog. Brain Res. 150, 127–142.
Rowland, N.C., Goldberg, J.A., Jaeger, D., 2010. Cortico-cerebellar coherence and causal connectivity during slow-wave activity. Neuroscience 166, 698–711.
Saitow, F., Murano, M., Suzuki, H., 2009. Modulatory effects of serotonin on GABAergic synaptic transmission and membrane properties in the deep cerebellar nuclei. J. Neurophysiol. 101, 1361–1374.
Schwarz, C., 2009. The fate of spontaneous synchronous rhythms on the cerebrocerebellar loop. Cerebellum 9, 77–87.
Sohal, V.S., Zhang, F., Yizhar, O., Deisseroth, K., 2009. Parvalbumin neurons and gamma rhythms enhance cortical circuit performance. Nature 459, 698–702.
Soteropoulos, D.S., Baker, S.N., 2006. Cortico-cerebellar coherence during a precision grip task in the monkey. J. Neurophysiol. 95, 1194–1206.
Soteropoulos, D.S., Baker, S.N., 2008. Bilateral representation in the deep cerebellar nuclei. J. Physiol. 586, 1117–1136.
Sugihara, L., Lang, E.J., Llinas, R., 1993. Uniform olivocerebellar conduction time underlies Purkinje cell complex spike synchronicity in the rat cerebellum. J. Physiol. 470, 243–271.
Van Wingerden, M., Vinck, M., Lankelma, J., Pennartz, C.M., 2010. Theta-band phase locking of orbitofrontal neurons during reward expectancy. J. Neurosci. 30, 7078–7087.
Weiss, M., Pellet, J., 1981. Modulation of harmaline-induced rhythmic discharge of the inferior olive by juxtafastigial stimulation. Brain Res. 215, 364–368.
Welsh, J.P., 1998. Systemic harmaline blocks associative and motor learning by the actions of the inferior olive. Eur. J. Neurosci. 10, 3307–3320.
Williams, E.R., Soteropoulos, D.S., Baker, S.N., 2009. Coherence between motor cortical activity and peripheral discontinuities during slow finger movements. J. Neurophysiol. 102, 1296–1309.
Williams, E.R., Soteropoulos, D.S., Baker, S.N., 2010. Spinal interneuron circuits reduce approximately 10-Hz movement discontinuities by phase cancellation. Proc. Natl. Acad. Sci. U. S. A. 107, 11098–11103.
Yarom, Y., Cohen, D., 2002. The olivocerebellar system as a generator of temporal patterns. Ann. NY Acad. Sci. 978, 122–134.
Zhang, X., Santaniello, S., 2019. Role of cerebellar GABAergic dysfunctions in the origins of essential tremor. Proc. Natl. Acad. Sci. U. S. A. 116, 13592–13601.